*Biochimica et Biophysica Acta*, 1060 (1991) 271–283



BBABIO 43502

# Kinetic modelling of exciton migration in photosynthetic systems. (1) Effects of pigment heterogeneity and antenna topography on exciton kinetics and charge separation yields *

Marc Beauregard, Iris Martin and Alfred R. Holzwarth

*Max-Planck-Institut für Strahlenchemie, Mülheim a.d. Ruhr (Germany)*

(Received 22 July 1991)

Key words: Fluorescence decay; Energy transfer kinetics; Photosynthesis; Chlorophyll fluorescence; Exciton migration; Kinetic model

**We report simulations of exciton migration and charge separation kinetics in spectrally heterogeneous two-dimensional model antenna/reaction center complexes based on a numerical solution of the Pauli master equation for exciton motion. Experimentally accessible quantities like the charge separation yield, the exciton lifetime(s), the first passage time, the time-resolved and the steady-state fluorescence emission spectra are calculated. The simulated data lend themselves to a direct comparison with experimental data. The diagnostic value of these parameters for studying antenna heterogeneity, antenna structure and trap properties in real photosystems are discussed. Both the 'slow trap' and the 'fast trap' cases are examined in order to simulate the trap-limited and the diffusion-limited kinetics, respectively. For spectrally heterogeneous antenna sytems we show that conclusions drawn by other authors regarding the effects of antenna optimisation like, e.g., funnelling, on the charge separation yield and exciton kinetics apply only to the hypothetical fast-trap case. In contrast, in the 'slow-trap case', which is more relevant for natural photosystems, the influence of spectral and structural optimization on the charge separation yield is quite limited. The most relevant parameters that influence the charge separation yield and the exciton kinetics in the heterogeneous antenna case are the ratio of energy transfer rates for trapping vs. detrapping at the reaction center and the spectral heterogeneity of the antenna. We show that the presence of long-wavelength-absorbing pigments (in relation to reaction center absorption) is still compatible with a high yield of charge separation. However, long-wavelength-absorbing pigments will make a pronounced contribution to the steady-state fluorescence emission spectrum, which has considerable diagnostic value. Funneling is shown to be essential for a short first passage time but less important for achieving a high yield of charge separation.**

## Introduction

In organisms performing photosynthesis, the light energy is absorbed by arrays of so-called 'antenna pigments' and is transferred in a series of ultrafast energy transfer steps to the photosynthetic reaction centers, the entities where the actual photoreactions take place (for reviews see Refs. 1, 2). Notwithstanding this generally accepted notion, most details of these energy transfer processes are still unknown. In fact, to date the energy transfer process in chlorophyll-containing antennae is neither experimentally nor theoretically understood, even for a single antenna pigment complex. This situation demands a substantial amount of both experimental and theoretical study.

The nonradiative transfer of excitation between antenna pigments in organisms performing photosynthesis was originally inferred from the concept of the photosynthetic unit. It was found that a large number of photochemically inactive antenna pigments are connected to one photoactive complex, the reaction center [3,4]. When Förster presented the exciton hopping theory on energy transfer in the very weak coupling limit [5] it was established that a random walk of the excitons over an array of pigment molecules including a trap could in principle be fast enough to ensure a

* Dedicated to Professor W. Wehrmeyer on the occasion of his 60th birthday.

Abbreviations: DAS, decay-associated spectrum; FPT, first passage time; RC, reaction center; PS, Photosystem; SWA, short-wavelength-absorbing; LWA, long-wavelength-absorbing.

Correspondence: A.R. Holzwarth, Max-Planck-Institut für Strahlenchemie, Stiftstrasse 34-36, D-4330 Mülheim a.d. Ruhr, Germany.

high energy-collection efficiency [6,7]. Theoretical modelling of the exciton motion in homogeneous arrays of pigments was first carried out on the basis of the probability matrix method [7], by establishing the master equations for exciton motion [8–12], or by Monte-Carlo random-walk simulations [13]. These studies provided fundamental insights into the energy-transfer processes on lattices containing traps. Nevertheless, the applicability of these studies to actual photosynthetic systems is limited, since some simplifying assumptions made, concerning the detailed properties of pigments and traps, seem to be incompatible with those of real photosystems.

A set of analytical expressions derived by Pearlstein [14] for the exciton lifetime in a homogeneous antenna array allowed for the first successful description of the kinetics of a photosynthetic unit with a realistic reversible trap. The predicted kinetics was a single-exponential decay function. That model was tested experimentally by Owens et al. [15] and it seems to be able to properly describe some basic aspects of the exciton decay kinetics in real photosystems. Pearlstein also discussed the origins of deviations from single-exponential exciton decay [16]. It was inferred that for a small charge separation rate the detailed properties of the antenna array should be of limited importance [14]. A major limitation of Pearlstein' s derivation is that only a spectrally homogeneous antenna system (all pigments are equal) can be considered and that only an average trapping lifetime is obtained.

Several numerical simulations of the exciton decay kinetics have been reported based on the probability matrix method [17–19], the Monte-Carlo random-walk method [13] or on the numerical integration of the master equation [20] and by other methods [21,22]. Despite providing interesting results, most of these studies were either highly restrictive in their assumptions (only homogeneous antenna and/or only irreversible traps assumed) or did not aim at calculating such parameters that could be compared directly with experimental data. A modelling of the exciton kinetics of large antenna systems composed of different pigment pools (heterogenous antenna) has been carried out in the past by using a coupled differential equation model. However, only the transfer between different pools of pigments was considered, ignoring the effects of the detailed pairwise transfer between all individual pigments [23,24]. The best-known of these models is Butler's tripartite model [25].

At present, a large variety of spectroscopic and kinetic data on photosynthetic antenna systems is available. Yet, most of the inherent structural and spectroscopic parameters governing the exciton motion in photosynthetic systems can not be revealed directly by an experimental spectroscopic approach alone. Kinetic modelling therefore promises to be a powerful approach to reveal these 'hidden parameters' of a particular antenna system. Such simulations should account as closely as possible for the multitude of experimental data that are available. No general analytical solution is available for this problem and thus numerical methods have to be applied.

The algorithm used here is based on the numerical solution of the Pauli master equation. This formalism allows us to simulate a variety of experimentally accessible data like, for example, the detailed fluorescence kinetics, the first passage time (FPT) the time-resolved decay-associated emission spectra (DAS), the steady-state emission spectrum, the fluorescence yield, the charge separation yield, etc., of a photosynthetic antenna/reaction center complex when the spectral properties, the spatial arrangement, and the energy transfer rates between individual pigments in the system are known. We have applied this approach earlier to a study of the energy transfer processes in phycobilisome rods [26] and a very similar formalism has been used in the work of Jean et al. [27]. Despite the fact that the method is not new, we are not aware of any complete presentation of the expressions required for the calculation of the experimentally accessible parameters described above. For this reason the necessary formulae are collected in the appendix of this paper.

The only systematic investigation of trapping kinetics in spectrally heterogeneous photosynthetic antenna systems published so far – using physically reasonable parameters for pigments and reaction centers – is that of Jean et al. [27]. They addressed two important topics in their study. First, the effects of spatial arrangement (in segregated antennae) and spatial distribution (in non-segregated antennae) on the exciton kinetics in model arrays was tested. Second, they addressed the problem of how – for a given spatial distribution – the corresponding simulated exciton kinetics would be 'seen' by a typical kinetic fluorescence experiment carried out using the single-photon-counting technique. The work reported here in a way complements and extends the work of Jean et al., although our aim is different. The main purpose of the present work is to investigate the effects of a varying degree of spectral heterogeneity on:

(i) the first-passage time in the antenna;
(ii) the total trapping kinetics and trapping yield; and
(iii) the effects of long-wavelength absorbing pigments on these parameters.

The important point in these simulations is that the degree of spectral heterogeneity is varied for a constant absorption spectrum of the array. In our view, this represents the typical experimental situation where one is trying to characterize an unknown antenna system in term of its spectral and spatial distribution and its kinetics. At the end of this paper we briefly compare the effects of different spatial arrangements for a

particular degree of spectral heterogeneity on the exciton kinetics. That part has significant relevance for understanding, for example, photosystem I. Throughout this work we aim at simulating as many experimental observables as possible in order to reveal their relationship with structural and spectral parameters of the antenna. In particular, we examine the effects of diffusion vs. trap-limited kinetics [14] in a coherent manner. We do not intend to meet exactly the properties of a particular natural photosynthetic system, although we believe that the assumed parameters are quite typical for Chl antenna systems of higher plants and green algae. Nevertheless, the results and insights gained in this study will be of a general nature and they will lay the ground for a detailed analysis of real photosystems – based on experimental data – which will be the subject of later work.

## Results

### *General model assumptions*

The antenna system considered consists of a regular two-dimensional array of pigments occupying $N-1$ lattice sites and in addition a trap. In our particular case, the trap is the so-called reaction center (RC). The deexcitation pathway of an excited antenna pigment can be energy transfer to a neighboring pigment (rate constant $k_{ij}$), radiative and nonradiative decay (summed together to give a rate constant $k_A$). The trap may or may not differ in its spectral properties from those of the antenna pigments. In any case, it is distinguished from the latter by an additional relaxation channel with rate constant $k_p$ reflecting irreversible charge separation. If not specified otherwise, only nearest-neighbor interactions will be considered for the energy transfer between pigments. The pairwise energy transfer rates, $k_{ij}$, are assumed to be proportional to the spectral overlap integral between donor and acceptor as defined in Förster energy transfer theory [28].

The rate constant $k_{ij}$ of transfer from pigment $j$ to pigment $i$ is thus given by

$$k_{ij} = \frac{\text{const} \cdot \kappa^2}{n^4 \cdot \tau_0 \cdot R_{ij}^6} \cdot O \tag{1}$$

with the spectral overlap integral $O$ being defined as

$$O = \int_\nu \frac{\epsilon_i(\nu) \cdot F_j(\nu)}{\nu^4} \mathrm{d}\nu \tag{2}$$

where $\kappa^2$ is the orientation factor, $n$ the refractive index, $\tau_0$ the radiative lifetime and $R_{ij}$ the distance between neighbouring pigments $i$ and $j$. $\epsilon_i(\nu)$ is the absorption spectrum of the acceptor pigment $i$ and $F_j(\nu)$ the normalized fluorescence spectrum of the donor pigment $j$.

For all the following simulations, a $9 \times 9$ square antenna array with the trap in the center will be assumed. The absorption spectra of the various pigments used were determined by Gaussian deconvolution of the total absorption spectrum into the desired number of spectral types. This assumed model spectrum was in fact the absorption spectrum of a PS II antenna reaction center complex which we have studied earlier [29]. The halfwidths of the bands in the Gaussian analysis were fixed. The fluorescence spectrum of each pigment type was assumed as the mirror image of the absorption with a fixed Stokes shift of 150 $cm^{-1}$. The number of pigments chosen of each spectral type was such that the total absorption spectrum (in the $Q_y$-band) of all model arrays represented an optimal fit of gaussian bands to the chosen experimental spectrum. Thus, within very small variations all simulated model arrays have the same total absorption in the $Q_y$ region but are composed of a varying number of different spectral types. For all model arrays the pigment–pigment distance was assumed to be 1.5 nm [30], $\epsilon_{max}^{abs} = 86300$ l/mol per cm [31], and an average orientation factor $\kappa^2$ of 5/4, which corresponds to a randomized orientation in two dimensions has been applied [32]. The rate constant for excited state deactivation $k_A$ (sum of radiative and nonradiative decays) was assumed to be 0.5 $ns^{-1}$, in accordance with a lifetime of approx. 2 ns in isolated Chl antennae [33–35], and the radiative lifetime $\tau_0 = 15$ ns [36]. The refractive index is 1.2. The trap (RC) is assumed to have identical spectral properties in all the simulated model arrays. It is characterized by a Gaussian absorption band with $\lambda_{max}^{abs} = 680$ nm (fwhm = 550 $cm^{-1}$), and a Gaussian emission band with $\lambda_{max}^{em} = 682$ nm (fwhm = 440 $cm^{-1}$). In general, we consider two types of RC as the trap. The first is a 'fast trap' with a charge separation rate constant of $k_p = 500$ $ps^{-1}$. This fast rate serves for the simulation of an irreversible trapping situation, since the charge separation rate is much larger than any energy transfer rate, so that charge separation occurs immediately after an exciton reaches the trap for the first time. The second type of RC considered has a slower, more realistic rate constant of charge separation of $k_p = 0.4$ $ps^{-1}$ ('slow trap'), which is in the range for a real reaction center [15,29,37–40]. This assumption allows us to switch between trap and diffusion limits without changing the pairwise energy transfer rate constants. This procedure provides a more realistic approach to the 'irreversible trapping' situation than the one used by previous authors who simply put to zero the back-transfer rate from the RC [17,19] which is a physically unreasonable assumption.

The excitation pulse was assumed to be a $\delta$-pulse at a wavelength of 675 nm (the maximum of the absorption) unless noted otherwise. We denote the longest lifetime predicted from the model calculation in each

case as $\tau_m$ with corresponding relative fluorescence amplitude $A_m$. The term 'maximal relative amplitude' of a lifetime component refers to the particular wavelength where the corresponding decay-associated spectrum (DAS, c.f. Appendix for definition) has a maximum. Since this maximum may occur at different wavelengths for the DAS of different decay components in the case of heterogeneous arrays, the sum of relative amplitudes of all components may in fact exceed a value of 100%. This definition may appear somewhat

TABLE I

*Results of simulations with heterogeneous antenna systems*

The position of the absorption maximum for each type is $\lambda_{max}^{abs}$, the emission maximum $\lambda_{max}^{cm}$, and the spectral width (fwhm) as calculated from the model array are given for each spectral type. $\tau_m$ and $A_m$ are the longest lifetime resolved and its relative amplitude, respectively, while $\phi_t$ represents the charge separation yield. The ratio $k_D/k_T$ is the ratio of energy transfer rate out of the trap to the transfer rate toward the trap. The other significant (in terms of amplitude) lifetime components and their corresponding amplitudes are given by $\tau_i$ and $A_i$. Kinetic analysis was made both for the fast ($k_p = 500$ ps$^{-1}$) and the slow ($k_p = 0.4$ ps$^{-1}$) trapping rate for excitation wavelength of 675 nm in all cases. RC, reaction center. The RC retained the same spectral properties throughout.

| Case | Type | #pigm | $\lambda_{max}^{abs}$ (nm) | fwhm (cm$^{-1}$) | $\lambda_{max}^{cm}$ (nm) | fwhm (cm$^{-1}$) | $k_p$ (ps$^{-1}$) | $\tau_m$ (ps) | $A_m$ | $\tau_i$ (ps) | $A_i$ | $\phi_t$ (%) | $k_D/k_T$ |
|---|---|---|---|---|---|---|---|---|---|---|---|---|---|
| A | 1 | 80 | 673 | 550 | 682 | 445 | 0.4 | 129 | 0.9998 | 0.124 | 0.001 | 93.5 | 0.65 |
| | RC | 1 | 680 | 550 | | | | | | | | | |
| | | | | | | | 500 | 6.2 | 0.978 | 0.338 | 0.01 | 99 | |
| B | 1 | 3 | 655.4 | 400 | 681 | 515 | 0.4 | 81.1 | 0.979 | 0.465 | 0.243 | 95.5 | 0.79 |
| | 2 | 37 | 667.5 | 400 | | | | | | 0.186 | 0.063 | | |
| | 3 | 24 | 677.8 | 400 | | | | | | 0.09 | 0.163 | | |
| | RC | 1 | 680.0 | 550 | | | | | | | | | |
| | | | | | 679 | 515 | 500 | 2.76 | 0.964 | 0.368 | 0.095 | 99 | |
| | | | | | | | | | | 0.294 | 0.009 | | |
| | | | | | | | | | | 0.181 | 0.042 | | |
| | | | | | | | | | | 0.082 | 0.122 | | |
| C | 1 | 7 | 655.5 | 350 | 686 | 780 | 0.4 | 174 | 0.728 | 1.11 | 0.323 | 92 | 1.56 |
| | 2 | 34 | 668.4 | 350 | + | | | | | 1.09 | 0.144 | | |
| | 3 | 37 | 679.3 | 350 | 705 | | | | | 0.296 | 0.237 | | |
| | 4 | 2 | 698.3 | 350 | | | | | | 0.113 | 0.108 | | |
| | RC | 1 | 680.0 | 550 | | | | | | | | | |
| | | | | | 685.5 | 750 | 500 | 5.1 | 0.758 | 1.08 | 0.445 | 99 | |
| | | | | | + | | | | | 1.1 | 0.27 | | |
| | | | | | 705 | | | | | 0.294 | 0.25 | | |
| | | | | | | | | | | 0.44 | 0.028 | | |
| D | 1 | 3 | 651.9 | 300.0 | 687 | 541 | 0.4 | 228 | 0.663 | 1.14 | 0.112 | 88 | 3.5 |
| | 2 | 11 | 661.0 | 300.0 | + | | | | | 0.927 | 0.225 | | |
| | 3 | 33 | 670.3 | 300.0 | 702 | | | | | 0.561 | 0.123 | | |
| | 4 | 30 | 680.4 | 300.0 | | | | | | 0.137 | 0.243 | | |
| | 5 | 3 | 695.5 | 300.0 | | | | | | | | | |
| | RC | 1 | 680.0 | 550.0 | | | | | | | | | |
| | | | | | 685 | | 500 | 6.94 | 0.633 | 1.79 | 0.017 | 99 | |
| | | | | | + | | | | | 1.27 | 0.086 | | |
| | | | | | 702 | | | | | 1.04 | 0.215 | | |
| | | | | | | | | | | 0.622 | 0.127 | | |
| E | 1 | 3 | 651.3 | 225 | 710 | 230 | 0.4 | 1550 | 0.36 | 8.70 | 0.22 | | |
| | 2 | 9 | 659.6 | | | | | | | 0.78 | 0.22 | 25 | 46 |
| | 3 | 20 | 667.4 | | | | | | | 0.65 | 0.14 | | |
| | 4 | 23 | 674.3 | | | | | | | 0.41 | 0.25 | | |
| | 5 | 20 | 682.7 | | | | | | | | | | |
| | 6 | 4 | 690.8 | | | | | | | | | | |
| | 7 | 1 | 702.0 | | | | | | | | | | |
| | RC | 1 | 680.0 | 550 | | | | | | | | | |
| | | | | | 710 | 230 | 500 | 248[a] | 0.28 | 5.67 | 0.22 | 93 | |
| | | | | | | | | | | 0.78 | 0.22 | | |
| | | | | | | | | | | 0.65 | 0.15 | | |
| | | | | | | | | | | 0.41 | 0.26 | | |

[a] Due to presence of a long-wavelength absorbing pigment (type 7), very long first-passage time.

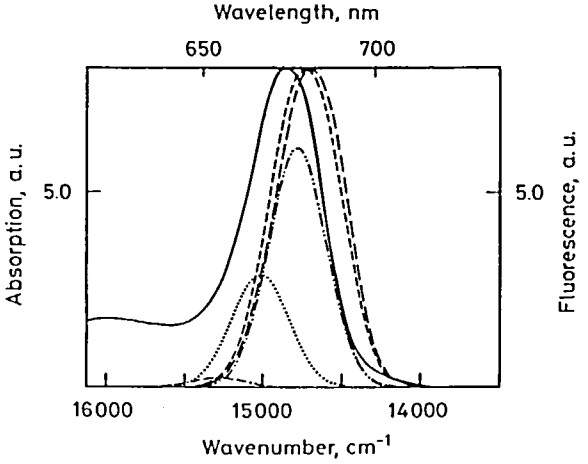


Fig. 1. Absorption spectra of pigment types (dotted and dash-dotted lines) and total absorption (solid line) used for simulating the heterogeneous 9×9 model array of case B (Table I). Type 1 (– – · – –), type 2 (· · · · · ·) and type 3 (– · · –). The calculated fluorescence spectra for case B are shown by the dashed lines for $k_p = 0.4$ ps$^{-1}$ (long dashes) and for $k_p = 500$ ps$^{-1}$ (short dashes). The Gaussian functions used to fit the first vibronic absorption side band around 640 nm are not shown for clarity.

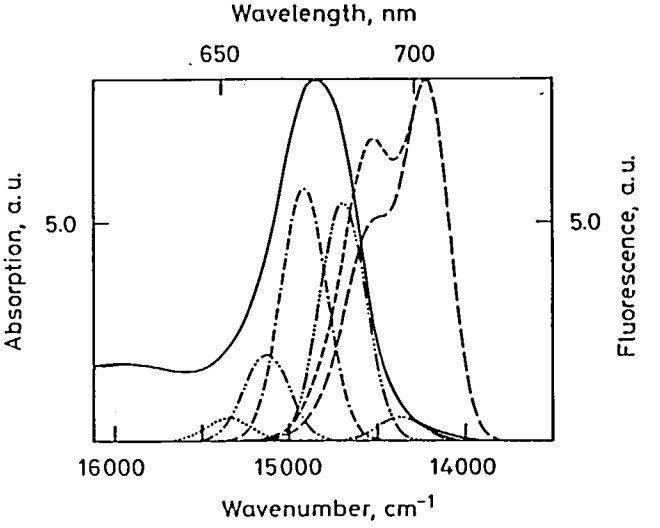


Fig. 3. Absorption spectra of pigment types used for simulating the heterogeneous 9×9 model array of case D (Table I). Type 1 (· · · · · ·), type 2 (– · · –), type 3 (– – · – –) type 4 (– · · · –) and type 5 (– · · –) absorption spectra are shown together with calculated emission spectra. For further symbols see Fig. 1.

unusual, but it allows us to condense the most important information contained in a particular DAS into a few numbers in a table.

For $N-1$ antenna pigments and 1 reaction center, the model predicts $N$ eigenvalues (lifetimes) and corresponding eigenvectors in the simulations. Since only a few of these eigenvectors have any significant magnitude, we shall ignore in the following discussion all those eigenvectors that make a negligible contribution to the total kinetics. We should like to note that several of these eigenvalues with significant eigenvectors may in fact represent rate constants with very similar values which in a real experiment could not be kinetically resolved. Nevertheless, we have not combined (or summed up) the corresponding DAS in order to enable a better understanding of the origin of these DAS. It would depend on experimental details how this kinetics would be 'seen' by an experimental procedure.

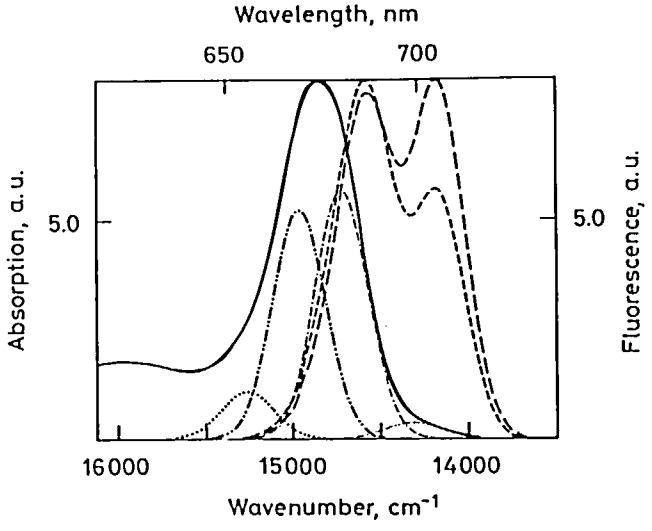


Fig. 2. Absorption spectra of pigment types used for simulating the heterogeneous 9×9 model array of case C (Table I). Type 1 (· · · · · ·), type 2 (– · · –), type 3 (– – · – –) and type 4 (· – · – ·) absorption spectra are shown together with the calculated emission spectra. For further symbols see Fig. 1.

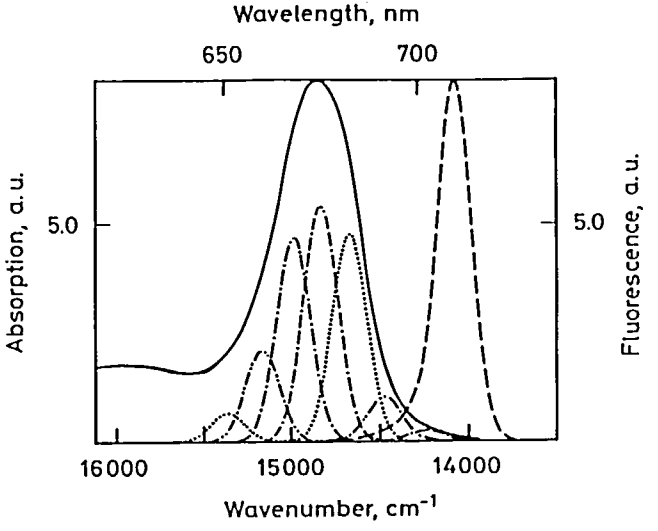


Fig. 4. Absorption spectra of pigment types used for simulating the heterogeneous 9×9 model array of case E (Table I). Type 1 (· · · · · ·), type 2 (– · · –), type 3 (· – · – ·),type 4 (– – · – –), type 5 (· · · · · ·), type 6 (– · · –) and type 7 (· – · – ·) absorption spectra are shown together with calculated emission spectra. For further symbols see Fig. 1. For this case the fluorescence spectra calculated with $k_p = 0.4$ ps$^{-1}$ or 500 ps$^{-1}$ are identical.

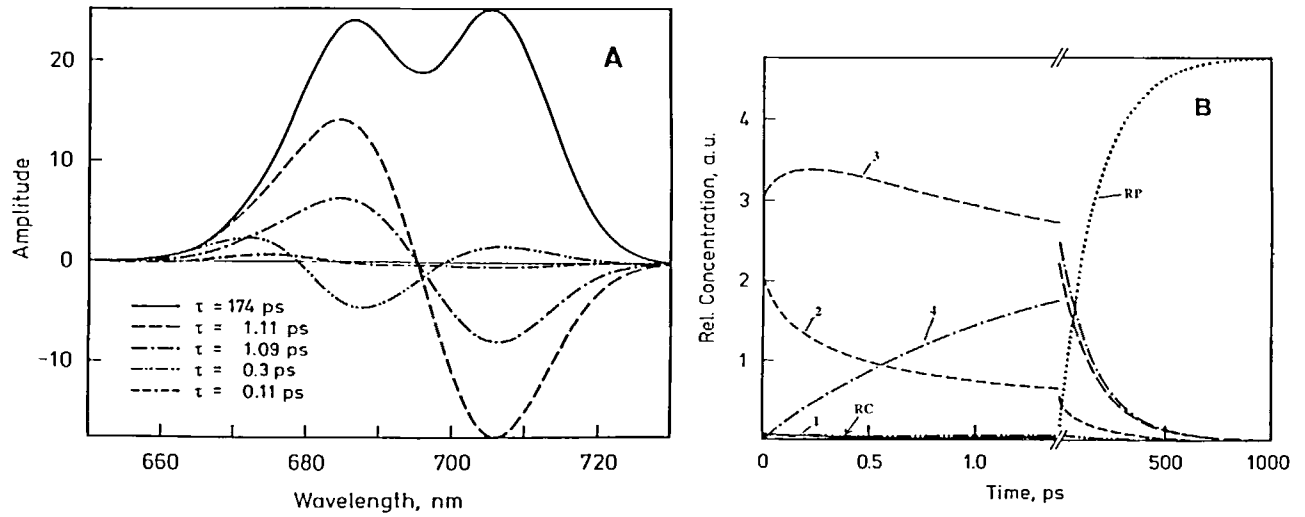


Fig. 5. (A) Decay associated spectra for the major lifetime components calculated for case C (Table I) assuming a slow trap and $\lambda_{exc} = 675$ nm. The DAS of the longest lifetime is almost identical with the predicted steady-state fluorescence spectrum. (B) Time dependence of the relative excited state concentrations of each pigment type for case C upon excitation at 675 nm. Numbers on curves denote the pigment types. RC reaction center; RP, charge separated state (radical pair). Note the split time-scale which is compressed after 1.4 ps. The symbols in panel A and panel B are not related to each other.

*Kinetic simulations*

We start out by studying the effect of an increasing degree of the antenna spectral heterogeneity on the exciton decay kinetics. After assuming a certain degree of spectral heterogeneity, characterized by a certain number of different spectral types and a particular pigment distribution, we calculate the overall trapping time and efficiency, the expected steady-state emission spectrum and the relative contribution of the fast lifetime component(s) which reflect the exciton equilibration kinetics between the different spectral types.

The results of the simulations assuming an increasing degree of spectral heterogeneity, modelled by an increasing number of different spectral types used, are collected in Table I. Unless noted otherwise, a funnel arrangement of the pigments has been applied, i.e., the longest-wavelength absorbing (LWA) pigments are located closest to the trap while the shortest-wavelength absorbing (SWA) pigments were placed at the periphery of the trap. For a given pigment ratio this rule alone does in most cases not fully determine the pigment arrangement. However, we verified that the alternative possibilities of arranging pigments within these limits, i.e., funnel arrangement, did not have severe influences on the results. A different approach would be to present an average of the kinetics of all possible funnel arrangements for a given pigment ratio. This would be incompatible, however, with the way we prefer to present the results for reasons of showing the principal effects. One must simply keep in mind that the cases presented in Table I are the result of one particular funnel arrangement each. Case A represents the homogeneous case with the same antenna size and is given for comparison only, while Cases B–E represent increasing degrees of heterogeneity. The absorption spectra of the different spectral types used are shown in Figs. 1–4.

*Fast trap case*

In the 'fast trap' ($k_p = 500$ ps$^{-1}$) case, the longest predicted lifetime, $\tau_m$, is found to be a good measure for the average arrival time of the exciton at the trap, i.e., the first passage time (FPT). The concept of the FPT has been defined in an analytical derivation by Montroll [9] and represents the time the excitons require on average to arrive for the first time at the trap (RC). Thus for $k_p = 500$ ps$^{-1}$ this decay time ($\tau_m$) should be identical to the first passage time (FPT) [14] since for $k_p \gg k_{ij}$, the exciton is converted into the charge separated state upon its first arrival at the RC. It is clear from inspection of Table I that increasing heterogeneity influences the longest lifetime component $\tau_m$ which has the predominant amplitude in all cases. However, this lifetime varies only from 2.8 ps (case B) to 6.9 ps (case D), which is much less than one might have expected intuitively. This small change in ($\tau_m$) is to the most extent explained by a decrease in the rate constant, $k_T$, which leads to a parallel increase in the ratio $k_D/k_T$ (the ratio of the rate constants for pairwise transfer from the reaction center to a neighboring antenna pigment, $k_D$, to the rate constant of the reverse process, $k_T$) upon increasing the degree of heterogeneity. * This in turn is related to the fact that

* We use here the ratio $k_D/k_T$ rather than the rate constant $k_T$ alone in order to be consistent with the 'slow trap case' where this ratio is a relevant parameter. We note however that the value of $k_D$ is not relevant in the 'fast trap case' considered in this paragraph.

for the highly heterogeneous cases considered there appear antenna pigments in the Gaussian deconvolution which have an absorption maximum at longer wavelength than the reaction center, i.e., energy transfer to the RC is energetically uphill. This is clearly born out by the results of case E. In this extreme case the FPT is nearly two orders of magnitude larger (FPT $\approx$ 250 ps) than for the other cases. For a reaction center that is a deep trap with respect to all the antenna pigments in the array the result would be different [17,41]. We have carried out the corresponding simulations for a 'deep trap' type of reaction center as well. The results are not presented here in detail because in our view such a situation is not likely to apply to any known antenna/reaction center complex in the physiological temperature range since the RC's seem to be always surrounded by pigments with similar or even lower excited state energy [20,42]. In the 'fast trap' case the trapping efficiency exceeds 93% in all cases. This holds even for case E, despite the fact that $k_T$ is quite unfavorable. This case may apply, for example, to purple bacteria like *Rhodospirillum rubrum* [42]. The data shows that in all cases the excitons quickly reach the RC and can be trapped efficiently.

*Slow trap case*

For the 'slow trap' case the overall trapping time – again characterized by the longest lifetime $\tau_m$ – is larger by more than an order of magnitude as compared to the FPT in the 'fast trap' case (cases A–D), as expected. It is interesting, however, that the overall trapping time is shorter as compared to the spectrally homogeneous antenna (case A) only for a modest degree of spectral heterogeneity (case B). For higher degrees of heterogeneity (cases C–E) the overall trapping time exceeds the 'homogeneous case' trapping time by up to a factor of 10. In all cases, except for very large degree of heterogeneity (case E) $\tau_m$ has a relative amplitude in the range 0.65–0.99. The other lifetimes have values $\leq 2$ ps, some of them having fairly large relative amplitudes of up to about 0.5 in some cases. This holds for an excitation wavelength at the maximum of the absorption of the whole array (675 nm). The short lifetimes reflect the antenna equilibration kinetics. Fig. 5A shows the DAS calculated for case C. The short lifetime ($\tau \approx 1$ ps) characterizes processes involving excitation decay in pigments emitting at 680–690 nm and a rise of excitation density in pigments emitting near 700–710 nm. The analysis of the time-dependence of excitation density for the four pigment types in the antenna indicates that an equilibration occurs between the excited state concentration in types 2 and 3 on the one hand and that in type 4 on the other hand within a time of 1–2 ps. Thus the emission maxima of these pigments agree with the positions of the predicted DAS maxima and minima. The third significant DAS with $\tau = 0.3$ ps is characterized by two decay components at 670 and 710 nm, and a rise term (negative amplitude) at 690 nm. Once again, examination of Fig. 5B reveals that a fast rise ($\tau < 1$ ps) the excited state population of type 3 pigments ($\lambda^{em}_{max} = 685$ nm) accounts for this DAS. The relative amplitude of these equilibration lifetimes increases with the degree of heterogeneity. It thus follows that the relative magnitude of the amplitudes of the equilibration components provides a good indicator for estimating the actual degree of spectral heterogeneity in an unknown antenna system.

Despite the large heterogeneity assumed, all the cases presented for the 'slow trap' assumption are extremely trap-limited, i.e., $\tau_m$ is strongly correlated with $k_p$. Nevertheless, the trapping yield (in our case

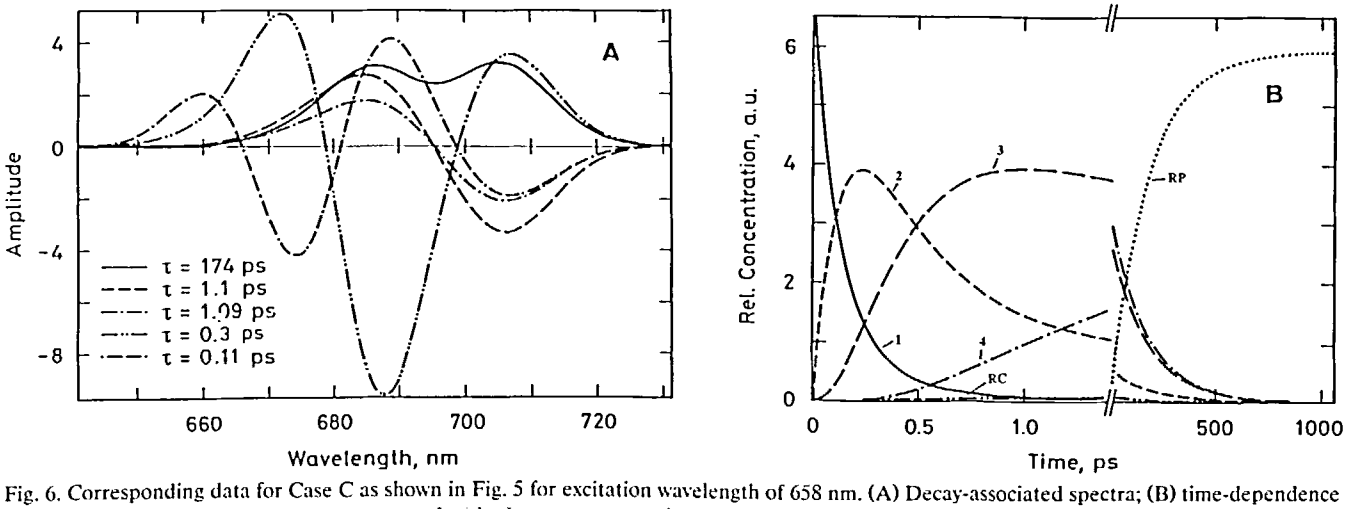


Fig. 6. Corresponding data for Case C as shown in Fig. 5 for excitation wavelength of 658 nm. (A) Decay-associated spectra; (B) time-dependence of excited state concentrations. For symbols see Fig. 5.

TABLE II

*Dependence of the maximal relative amplitude, $A_i$ of lifetime component $\tau_i$ on the excitation wavelength $\lambda_{exc}$ for the heterogeneous cases B–E with $k_p = 0.4\ ps^{-1}$ (c.f. Table I)*

Values for charge separation yield $\phi_t$ are not sensitive on excitation wavelength.

| Case | $\tau_i$ (ps) | $\lambda_{exc}$ (nm) | $A_i$ | $\lambda_{exc}$ (nm) | $A_i$ | $\lambda_{exc}$ (nm) | $A_i$ |
|---|---|---|---|---|---|---|---|
| B | 81.1 | 655 | 0.844 | 675 | 0.979 | 679 | 0.995 |
| (3 types) | 0.47 | | 0.424 | | 0.243 | | 0.004 |
| | 0.30 | | 0.014 | | 0.008 | | 0.002 |
| | 0.19 | | 0.026 | | 0.063 | | 0.020 |
| | 0.09 | | 0.470 | | 0.163 | | 0.156 |
| C | 174 | 658 | 0.262 | 675 | 0.728 | 698 | 0.906 |
| (4 types) | 1.11 | | 0.181 | | 0.323 | | 0.098 |
| | 1.09 | | 0.115 | | 0.144 | | 0.043 |
| | 0.30 | | 0.364 | | 0.237 | | 0.242 |
| | 0.11 | | 0.132 | | 0.108 | | 0.072 |
| D | 228 | 652 | 0.172 | 675 | 0.663 | 695 | 0.952 |
| (5 types) | 1.14 | | 0.046 | | 0.112 | | 0.034 |
| | 0.93 | | 0.08 | | 0.225 | | 0.100 |
| | 0.56 | | 0.095 | | 0.123 | | 0.071 |
| | 0.20 | | 0.121 | | 0.069 | | 0.073 |
| | 0.1247 | | 0.345 | | 0.243 | | 0.1875 |
| E | 1550 | 651 | 0.02 | 675 | 0.36 | 702 | 0.96 |
| (7 types) | 8.7 | | 0.006 | | 0.22 | | 0.35 |
| | 0.78 | | 0.018 | | 0.22 | | 0.042 |
| | 0.65 | | 0.005 | | 0.14 | | 0.025 |
| | 0.41 | | 0.010 | | 0.25 | | 0.213 |
| | 0.119 | | 0.212 | | 0.085 | | 0.017 |

TABLE III

*Effect of pigment spatial arrangement on exciton decay in a heterogenous antenna (pigment composition as in Case D from Table I)*

The exact arrangement of pigments is shown in Fig. 7. Case D1 is the control funnel array; cases D3-D4 are nearly funnel arrays where the position of the pigment type 5 is modified; case D2 has a nearly anti-funnel arrangement near the trap. Cases D5, D6 and D7 have a computer-generated random distribution of pigments in the array. The presence of positive/negative amplitude components in the DAS is noted by +/−. Other parameters are as described in Table I. (The values in parentheses give the intensity of the corresponding maximum relative to the total maximum of the emission spectrum.)

| Case | $\lambda_{max}^{em}$ [nm] | $\tau_i$ [ps] | $A_i$ | DAS | $\phi_t$ [%] | $k_D/k_T$ | FPT ($k_p = 500$) |
|---|---|---|---|---|---|---|---|
| D1 | 687 (0.6) | 228 | 0.663 | + | 88 | 3.5 | 6.9 |
| | 702 | | | | | | |
| D2 | 687 (0.6) | 276 | 0.664 | + | 85 | 0.14 | 59.6 |
| | 702 | | | | | | |
| D3 | 687 (0.15) | 159 | 0.549 | + | 78 | 2.0 | 5.8 |
| | 702 | 2000 [a] | 0.130 | +/− | | | |
| D4 | 687 (0.05) | 51 | 0.928 | +/− | 50 | 1.1 | 3.2 |
| | 702 | 2000 [a] | 0.6 | + | | | |
| D5 | 687 (0.2) | 182 | 0.587 | + | 76 | 0.4 | 35.0 |
| | 702 | 20.6 | 0.189 | +/− | | | |
| | | 2000 [a] | 0.142 | + | | | |
| D6 | 687 (0.5) | 328 | 0.546 | + | 87 | 0.55 | 32.4 |
| | 702 | 462 | 0.178 | +/− | | | |
| | | 97.7 | 0.154 | + | | | |
| D7 | 687 (0.6) | 254 | 0.65 | + | 87 | 0.6 | 40.6 |
| | 702 | 1.91 | 0.21 | +/− | | | |

[a] In this arrangement at least one long-wavelength (LWA) pigment which is surrounded by short-wave-pigments only, acts as a second trap.

identical to the charge separation yield) is very high, i.e., 88–95% for all cases except case E. This shows that the presence of long-wavelength absorbing pigments is quite compatible with a high trapping yield. Only for case E, where the presence of an extremely low-energy antenna pigment (as compared to the energy of the RC) is assumed, does the trapping yield drop drastically to 25%. Increasing heterogeneity has also a drastic influence on the predicted steady-state emission spectra, as shown in Figs. 1–4. For increasing heterogeneity the emission spectrum develops a red emission band ($\lambda_{em}$ = 700–706 nm) whose intensity increases relative to the 680–685 nm main emission band. This demonstrates convincingly that the maximum and shape of the steady-state emission spectrum should in fact provide a simple but important criterion when judging the degree of spectral heterogeneity in a natural system.

*Dependence on excitation wavelength*

The relative amplitudes of the fast equilibration lifetimes are expected to depend strongly on the excitation wavelength [26] (note that the lifetimes are independent of excitation wavelength). Thus calculations assuming excitation at two other wavelengths, i.e., at the maxima of the shortest- and longest-wavelength-absorbing antenna pigment, respectively, were performed in addition to the 675 nm excitation assumed normally. The maximal relative amplitudes are collected in Table II. It follows from these results that the variation in the DAS of the short-lived components observed for different excitation wavelengths are not only potent indicators for the spatial and spectral equilibration kinetics in the heterogeneous antenna but also provide insight into the spectral characteristics of the different pigment pools. As an example, the resulting DAS for case C and $\lambda_{exc}$ = 658 nm are shown in Fig. 6A. This figure should be compared with Fig. 5A, which shows the corresponding data for the same array but using $\lambda_{exc}$ = 675 nm. As a result of the blue-shifted excitation, the rel. amplitudes of the two shortest lifetimes increase substantially. The shortest $\tau$ shows a decay term at 660 nm, which suggests a decrease of excited state population of the type 1 pigments with $\tau$ = 0.14 ps. In accordance with this, excited state concentration curves reveal a fast equilibration ($\tau$ < 0.5 ps) involving decay of type 1 excited states and simultaneous rise of type 2 excited state population (see Fig. 6B).

*Effects of pigment distribution*

Table III collects the results obtained when studying the dependence of the trapping parameters for an intermediate degree of spectral heterogeneity as a function of spatial arrangement in the 'slow trap' case. We chose the same pigment ratio as in case D, Table I. The complete funnel arrangement (case D1, identical to case D, Table I) is compared with various non-random nearly-funnel (D3, D4) or nearly anti-funnel (D2) and also with several computer-generated random arrangements (D5-D7). The exact arrangement of the pigments used for these simulations is shown in Fig. 7. In the case of the random arrangements we show the results of extreme cases (D5 and D7) as well as a case which is more typical for the average kinetics (D6). For some arrangements (case D3, D4, D5) one of the LWA pigments is located far away from the RC and is

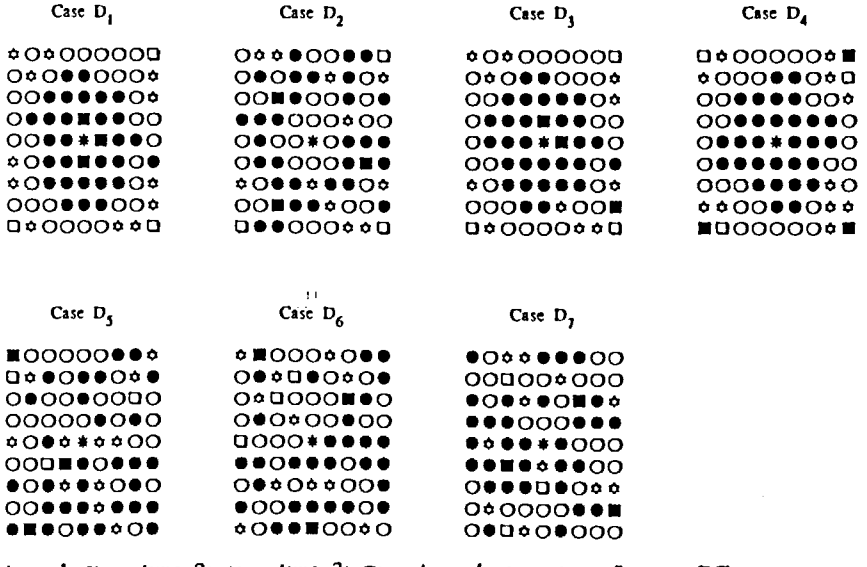


Fig. 7. Model lattices having the pigment type distribution of case D (Table I) but different pigment arrangement in the array. Funnel (D1), nearly anti-funnel (D2) nearly funnel (D3-D4) and random (D5-D7) arrangements are shown.

surrounded by SWA pigments. The LWA pigments thus act as an additional trap, which gives rise to a substantial 2 ns decay amplitude, because energy being directed to these pigments never finds its way back to the RC. Consequently, the trapping efficiency drops considerably, to a value as low as 50%. For the other pigments the trapping time is very short (51 ps for case D4). For the random arrangements (D5-D7) and for the anti-funnel arrangement (D2) the FPT is by a factor of 5–10 higher than for the other cases, extending up to about 60 ps.

Comparison of the FPT for all distributions reveals that funneling of excitation as realized in cases D1, D3, and D4, is highly efficient in reducing the exciton migration time to the RC. For the other cases the FPT is increased, up to 60 ps for the anti-funnel case D2. This effect of funnelling has been predicted earlier [17,19]. The important point is, however, that it has no corresponding effect on the trapping time and the charge separation yield when $k_p = 0.4\ ps^{-1}$, i.e., for a realistic trap. In fact, cases D2 and D7 (random distribution) are now characterized by similar trapping times, charge separation yield and fluorescence spectra as found in the best case, D1. We furthermore find that, independent of funneling, the environment of the LWA pigments has a decisive impact on the exciton migration kinetics. The cases D3 and D4 reveal that moving from 1 to 3 LWA pigments to the edge of the array, the ratio $k_D/k_T$, the FPT and the RC-controlled trapping time are decreased. However, this apparent positive effect is accompanied by the appearance of a 2 ns component of substantial amplitude, a drastic increase in long-wavelength, 702 nm fluorescence and moreover a decrease of trapping yield down to 50%. Similar results are obtained also for case D5. It had been concluded previously that LWA pigments should not be located near the trap, since the increase of $k_D$ by LWA pigments should decrease the trapping efficiency [14,20]. Our simulation reveals that such a conclusion is inappropriate. The LWA pigments must clearly be in contact with the trap, otherwise no high trapping efficiency can be achieved. LWA pigments not in contact with the trap tend to act as additional traps where energy becomes localized and thus can not reach the reaction center efficiently. It follows from these studies that the pigment distribution in an inhomogeneous antenna array can be quite variable without affecting a high charge separation yield. The only limiting factor is the environment of the LWA pigments. If LWA pigments (relative to the RC absorption) should be part of real photosystems we conclude that they should be preferentially situated close to the reaction center.

The shape of the steady-state emission spectra is a sensitive parameter for the pigment arrangement, as is revealed by the intensity ratio of the 687 nm to the 702 nm emission intensity (Table III). The simulations presented here show that in fact only for the funnel array D1 and few other cases (D2 and D7) the fluorescence intensity of the LWA pigments at 702 nm is similar to the fluorescence intensity of the 687 nm band. For the cases D3-D5 where the LWA pigments are obviously not located at the end of an energetic funnel leading to the reaction center, the fluorescence from the LWA pigments is highly enhanced. It appears that a random distribution of the pigments does not necessarily decrease exciton density in the LWA pigments as was suggested previously [43]. In fact, for comparable trapping times and fluorescence spectra (like cases D1, D2 and D7) only the FPT can be used as a criterion to distinguish a perfect funnel array from other arrangements. Although we have not tried intentionally to model the situation for PS I, we should like to note that in fact cases D3-D7 have many similarities with the properties of PS I particles, in particular with respect to a small number of LWA pigments involved. Lifetimes of 10–20 ps observed in both isolated PS I particles [44–46] and in intact thylakoids and green algae (see Ref. 47 for a review) have been interpreted by us as spectral and spatial antenna equilibration times. Taking into account that native PS I antenna have antenna sizes about 2–3-times larger than the arrays simulated here, our interpretation of the abovementioned experimental data is entirely consistent with the results from the simulations reported here. In that case, the relative arrangement of LWA pigments and RC is particularly important.

## Discussion

Our simulations show that only an exact solution of the equations describing the exciton kinetics as carried out here can give information about the influence of spectral heterogeneity in antenna pigments on the trapping kinetics and yields. Previous formalisms limited to homogeneous systems led to wrong conclusions in this regard if extrapolated to the heterogeneous cases. The dependence on $k_D$ and $k_T$ which is important in a homogeneous system [14,20] may be overriden by funnelling in a heterogeneous one. It is clear from our simulations that the presence of LWA pigment can be an advantage for the trapping efficiency in special cases but does not generally improve the efficiency.

Previous simulations where spectral heterogeneity was examined in detail are inconclusive for real systems because their predictions were mostly limited to the effect on the FPT [17,19]. Our data show that FPT alone does not constitute a relevant parameter for characterizing the exciton decay kinetics and yield of trapping when a realistic 'slow trap' situation is modelled. For example the improvement of trapping efficiency by heterogeneity, predicted to decrease trapping

time by a factor of 2–5, was in fact only about 35% in the best case studied here. It thus appears that the most relevant characteristics of a funnel arrangement compared to other arrangements consists in the decrease in FPT and in the minimized fluorescence emission from the LWA pigments, although it does not necessarily provide a substantially better trapping efficiency. Thus, considering only the effects on the FPT and the ratio $k_D/k_T$ may be misleading if the trapping efficiency is not considered as well [19,20]. It is also worth mentioning that there exists no obvious relationship between the steady-state fluorescence spectra and the spectra of the pigment families present in the antenna. The full kinetics of the antenna system including the trap must be solved exactly in order to predict such fluorescence emission. Any intuitive predictions concerning the performance of a given array are likely to fail due to the complexity of the exciton kinetics involved in a heterogeneous antenna with a slow, reversible trap. This situation provides a useful handle, however, for learning about the spectral heterogeneity and the spatial distribution of natural antenna systems. One important conclusion to be drawn here is that previous reports, limiting their investigation to the FPT [17,19], largely overestimated the importance of the positive impact of a complete funnel arrangement as compared to other pigment distributions on the trapping efficiency.

At this point a comparison with the results of the study by Jean et al. [27] is appropriate. When making such comparison it must be kept in mind that Jean et al. presented their data in a manner quite different from that followed by us. They calculated the simulated kinetics with a time interval of 5 ps and performed a sum-of-exponentials analysis on these data. In contrast, we present directly the lifetimes (inverse eigenvalues ) and the DAS (from the eigenvectors) of the respective kinetic system. Jean et al. also did not calculate the FPT and the trapping yield. The most important common conclusion to be drawn from the two studies are the following:

(i) Both predict that kinetic components in the range from subpicoseconds up to a few picoseconds will contain the most relevant information both on the spatial distribution as well as on the degree of spectral heterogeneity of the antenna systems.

(ii) The equilibration times (spectral and spatial) are not directly related to the overall trapping time and yields (for realistic slow traps).

(iii) The excitation or emission spectrum of the trapping sensitive lifetime, $\tau_m$, is identical to the corresponding steady state spectrum (for slow traps). The last conclusion follows already from the work on phycobilisomes [26]. A further detailed comparison of the results is difficult in view of the different parameters that were varied in the two studies. Nevertheless it can be concluded that in general the results of both studies are quite compatible with each other.

Our study provides useful insight on how time-resolved fluorescence spectroscopy could be used in the most informative way to reveal so far unexplored details of antenna structure and the properties of natural photosystems. We conclude that the deviation of the exciton kinetics from the monoexponential decay, the appearance of shorter-lived components and their DAS in dependence on the excitation wavelength, and last but not least the steady-state fluorescence spectra are all sensitive indicators of the spectral heterogeneity and the actual pigment arrangement present in a photosystem. In order to exploit this potential, subpicosecond studies of antenna equilibration will have to be carried out.

**Acknowledgements**

This work has been supported by a postdoctoral fellowship to M.B. from the Natural Sciences and Engineering Research Council of Canada. We thank Professor K. Schaffner for his interest in and support of this work.

**Appendix**

*Description of the formalism*

Assuming that exciton motion is an incoherent hopping process of localized excitons, and assuming low photon densities (one exciton created per domain only) the exciton motion in a system of n pigments is described by the Pauli master equation [5], which for practical purposes is equivalent to a random-walk formulation [48]:

$$\frac{dx_i}{dt} = \left( -k_{0i} - \sum_{\substack{j=1 \\ j \neq i}}^{n} k_{ij} \right) x_i + \sum_{\substack{j=1 \\ j \neq i}}^{n} k_{ij} x_j ; \; i = 1 \ldots n \qquad \text{(A-1)}$$

In matrix notation this can be written as (vectors and matrices in bold symbols):

$$\dot{\boldsymbol{x}} = \boldsymbol{T}\boldsymbol{x} + \boldsymbol{b}e(t)$$

where $\dot{x}$ is the time derivative vector of the occupation probabilities $x$ for the $n$ species, $T$ is the transfer matrix for which the elements are defined as:

$$t_{ij} = (1 - \delta_{ij}) k_{ij} - \delta_{ij} \left( k_{0i} + \sum_{\substack{r=1 \\ r \neq j}}^{n} k_{rj} \right) \qquad \text{(A-2)}$$

where the $k_{ij}$ and $k_{0i}$ are the rate constants for exciton transfer or electron transfer and deactivation to the ground state, respectively. The term $be(t)$ is defined by the initial conditions, where $b$ is the vector of time

zero absorbancies for all species and $e(t)$ is the excitation function which is assumed to be a $\delta$-function in our calculations. The term $Tx$ describes the intrinsic time dependence of the system.

The system of homogeneous linear differential equation $\dot{x} = Tx$ is solved by the expression

$$x = u \cdot \exp(\gamma t)$$

thus,

$$\dot{x} = \gamma \cdot u \cdot \exp(\gamma t) \tag{A-3}$$

and replacing $\dot{x}$ and $x$ in $\dot{x} = Tx$ we find

$$Tu = \gamma u \tag{A-4}$$

which is an eigenvalue problem that is solved by $n$ eigenvalues $\gamma_i$ and their corresponding eigenvectors $u_i$. In vector space notation, the solutions are thus given by:

$$x(t) = \sum_{i=1}^{n} d_i \cdot u_i \cdot \exp(\gamma_i t) \tag{A-5}$$

where $d_i (i = 1, 2, \ldots, n)$ are scalars defined by the initial excitation conditions. They are determined by the concentration of each ground state species at $t = 0$, their absorption spectra and the excitation wavelength used. All these parameters are included in the term $b \cdot e(t)$. Thus at $t = 0$, $x(0) = b$ and we have:

$$x(0) = \sum_{i=1}^{n} d_i u_i = b = Ud \tag{A-6}$$

where $U$ is the matrix of eigenvectors $u_i$, $i = 1, 2, \ldots, n$. Hence, $d = U^{-1} b$
Having defined $d$, we then write:

$$x(t) = \sum_{i=1}^{n} u_i^* \cdot \exp(\gamma_i t) \tag{A-7}$$

where $u_i^* = d_i u_i$ is the 'initial condition scaled' eigenvector for the eigenvalue $\gamma_i$.

*Calculation of experimentally observable data*

Let us assume that the exciton motion is followed by a kinetic fluorescence experiment, where $f(t)$ is the experimental fluorescence time course, as a function of excitation and emission wavelengths. According to Eqn. A-7 this will be a multi-exponential decay with $N$ terms:

$$f(\lambda_{exc}, \lambda_{em}, t) = \sum_{i=1}^{n} a(\lambda_{exc}, \lambda_{em})_i \cdot \exp(-t/\tau_i) \tag{A-8}$$

The lifetimes $\tau_i$ are equal to the negative reciprocal eigenvalues ($\tau_i = -\gamma_i^{-1}$), while the amplitudes corresponding to the lifetime component $\tau_i$ are given by the vector $a_i$

$$a_i = F \cdot u_i^* \tag{A-9}$$

where $F$ is a matrix formed by all vectors describing the fluorescence spectra of all pigments as a function of emission wavelength $\lambda_{em}$. The vector $a_i$ is called the decay-associated spectrum (DAS) of lifetime component $\tau_i$ and it is in principle directly experimentally accessible, provided the measuring system has enough time resolution. The DAS and $\tau_i$ contain all the information that can be obtained in an isotropic time-resolved fluorescence experiment.

In a similar way, the stationary fluorescence spectrum $L$ represented in vector notation is obtained

$$L = \sum_{i=1}^{n} a_i \cdot \tau_i \tag{A-10}$$

Thus, we are able to calculate all relevant experimental parameters once the excitation conditions, the absorption and emission spectra of individual pigments, the pigment composition and arrangement, and the rate constants for transfer are given.

## References


1 Parson, W.W. and Ke, B. (1982) in Primary Photochemical Reactions. in Photosynthesis (Govindjee, ed.), Vol. 1, pp. 331–385. Academic Press, New York.
2 Cogdell, R.J. (1983) Annu. Rev. Plant Physiol. 34, 21–45.
3 Emerson, R. and Arnold, W. (1932) J. Gen. Physiol. 16, 191–205.
4 Duysens, L.N.M. (1952) Ph.D. thesis, University of Utrecht, The Netherlands.
5 Förster, T. (1948) Ann. Phys. Leipzig 2, 55–75.
6 Bay, Z. and Pearlstein, R.M. (1963) Proc. Natl. Acad. Sci. USA 50, 1071–1078.
7 Robinson, G.W. (1967) Brookhaven Symp. Biol. 19, 16–48.
8 Knox, R.S. (1968) J. Theor. Biol. 21, 244–259.
9 Montroll, E.W. (1969) J. Math. Phys. 10, 753–765.
10 Pearlstein, R.M. (1967) Brookhaven Sym. Biol. 19, 8–15.
11 Kenkre, V.M. and Knox, R.S. (1974) Phys. Rev. B 9, 5279–5290.
12 den Hollander, W.T.F., Bakker, J.G.C. and Van Grondelle, R. (1983) Biochim. Biophys. Acta 725, 492–507.
13 Altmann, J.A., Beddard, G.S. and Porter, G. (1978) Chem. Phys. Lett. 58, 54–57.
14 Pearlstein, R.M. (1982) Photochem. Photobiol. 35, 835–844.
15 Owens, T.G., Webb, S.P., Mets, L., Alberte, R.S. and Fleming, G.R. (1987) Proc. Natl. Acad. Sci. USA 84, 1532–1536.
16 Pearlstein, R.M. (1984) in Advances in Photosynthesis Research (C. Sybesma eds.). Vol. 1, pp. 13–20. Nijhoff, The Hague.
17 Seely, G.R. (1973) J. Theor. Biol. 40, 173–187.
18 Seely, G.R. (1973) J. Theor. Biol. 40, 189–199.
19 Fetisova, Z.G., Borisov, A.Y. and Fok, M.V. (1985) J. Theor. Biol. 112, 41–75.
20 Shipman, L.L. (1980) Photochem. Photobiol. 31, 157–167.
21 Borisov, A.Y. (1987) Biophysics 32, 1139–1157.
22 Borisov, A.Y. (1990) Photosyn. Res. 23, 283–289.
23 Freiberg, A., Godik, V.I., Pullerits, T. and Timpman, K. (1989) Biochim. Biophys. Acta 973, 93–104.

24 Geacintov, N.E., Breton, J. and Knox, R.S. (1986) Photosyn. Res. 10, 233–242.
25 Butler, W.L. (1978) Annu. Rev. Plant Physiol. 29, 345–378.
26 Suter, G.W. and Holzwarth, A.R. (1987) Biophys. J. 52, 673–683.
27 Jean, J.M., Chan, C.-K., Fleming, G.R. and Owens, T.G. (1989) Biophys. J. 56, 1203–1215.
28 Förster, T. (1965) in Modern Quantum Chemistry (Sinanoglu, O. ed.), Part III, pp. 93–137, Academic Press, New York.
29 Schatz, G.H., Brock, H. and Holzwarth, A.R. (1988) Biophys. J. 54, 397–405.
30 Beddard, G.S. and Porter, G. (1976) Nature 260, 366–367.
31 Seely, G.R. (1966) in The Chlorophylls (Vernon, L.P., ed.). pp. 523–568, Academic Press, New York.
32 Campillo, A.J., Hyer, R.C., Monger, T.G., Parson, W.W. and Shapiro, S.L. (1977) Proc. Natl. Acad. Sci. USA 74, 1997–2001.
33 Nordlund, T.M. and Knox, W.H. (1981) Biophys. J. 36, 193–201.
34 Ide, J.P., Klug, D.R., Kühlbrandt, W., Giorgi, L.B. and Porter, G. (1987) Biochim. Biophys. Acta 893, 349–364.
35 Eads, D.D., Webb, S.P., Owens, T.G., Mets, L., Alberte, R.S. and Fleming, G.R. (1987) in Progress in Photosynthesis Res. (Biggins, J. ed.), Vol. I, pp. 135–138. Nijhoff, Dordrecht.
36 Persson, B.N.J. (1986) Chem. Phys. Lett. 128, 107–112.
37 Woodbury, N.W., Becker, M., Middendorf, D. and Parson, W.W. (1985) Biochemistry 24, 7516–7521.
38 Martin, J.-L., Breton, J., Hoff, A.J., Migus, A. and Antonetti, A. (1986) Proc. Natl. Acad. Sci. USA 83, 957–961.
39 Holzapfel, W., Finkele, U., Kaiser, W., Oesterhelt, D., Scheer, H., Stilz, H.U. and Zinth, W. (1989) Chem. Phys. Lett. 160, 1–7.
40 Wasielewski, M.R., Johnson, D.G., Seibert, M. and Govindjee (1989) Proc. Natl. Acad. Sci. USA 86, 524–528.
41 Fetisova, Z.G., Shibaeva, L.V. and Fok, M.V. (1989) J. Theor. Biol. 140, 167–184.
42 Van Grondelle, R., Bergström, H., Sundström, V. and Gillbro, T., (1987) Biochim. Biophys. Acta 894, 313–326.
43 Owens, T.G., Webb, S.P., Alberte, R.S., Mets, L. and Fleming, G.R. (1988) Biophys. J. 53, 733–745.
44 Holzwarth, A.R., Haehnel, W., Ratajczak, R., Bittersmann, E. and Schatz, G.H. (1990) in Current Research in Photosynthesis (Baltscheffsky, M., ed.), Vol. 2, pp. 611–614, Kluwer, Dordrecht.
45 Holzwarth, A.R. (1990) in Current Research in Photosynthesis (Baltscheffsky, M., ed.), Vol. 2, pp. 223–230, Kluwer, Dordrecht.
46 McCauley, S.W., Bittersmann, E., Müller, M.G. and Holzwarth, A.R., (1990) in Current Research in Photosynthesis (Baltscheffsky, M., ed.), Vol. 2, pp. 297–300. Kluwer, Dordrecht.
47 Holzwarth, A.R. (1991) in Chlorophylls (Scheer, H., ed.), pp. 1125–1151, CRC Press, Boca Raton.
48 Hemenger, R.P., Pearlstein, R.M. and Lakatos-Lindenberg, K. (1972) J. Math. Phys. 13, 1056–1063.